Modeling process damping via FEM based Force-FRF

Daniel BACHRATHY, Attila KOSSA, Gabor STEPAN
Department of Applied Mechanics, Budapest University of Technology and Economics, Műegyetem rkp 3, Budapest H-1111, Hungary
bachrathy@mm.bme.hu, kossa@mm.bme.hu, stepan@mm.bme.hu

Abstract: To reach the maximal material removal rate in turning processes, optimal technological parameters can be selected from the corresponding stability charts. At low cutting speed ranges, appropriate modeling of the process damping effect is essential to obtain reliable stability charts. Large variety of physical explanations and mathematical descriptions are used in the literature to predict the increased stability limits in the corresponding parameter domains.

In this study, the cutting force is calculated by means of finite element method (FEM) based simulations. Due to the surface regeneration effect, the cutting force depends on the current and the delayed tool positions. This complex dependency is modeled separately with the help of two different frequency response functions (FRF). The first FRF is based on the time signal of the cutting force computed by FEM for a predefined perturbed tool motion. The second one is obtained by introducing a perturbed surface profile which also affects the resultant cutting force. The combination of these two FRFs presumably includes all the relevant sources of the process damping phenomenon, such as the contact forces on the flank face, the short regenerative effect on the rake face, and also the plastic deformation, thermal effects at the tool tip. Stability charts are constructed based on these specific FRFs for a single degree-of-freedom mechanical model. It is shown, that the process damping phenomenon can be explained via different physical effects and that they all have similar influences on cutting stability.

Keywords: stability, FEM, chip formation, process damping.

1. INTRODUCTION

For turning processes experience shows, that the lower envelope of stability lobes in the low spindle speed range shifts up to higher depth of cut values. There exist various models to describe this phenomenon. In a widely spread model, so-called process damping model, additional damping proportional to the time delay is added to the structural damping to characterize the contact force at the small region between the flank face and the work piece ([Das and Tobias, 1967], [Chiou et al., 1998], [Altintas et al., 2008] and [Eynian, 2010]).

A different explanation is given in [Stépán,1984] and [Stépán, 1989], where the contact force on the rake face is modeled by a short delay representation.

The main goal of this study is to give a model for the cutting force including all relevant sources of the phenomenon explained above. The force fluctuation caused by the current tool motion and by the motion of the tool one revolution before is simulated by means of FEM computations.

2. MECHANICAL MODEL

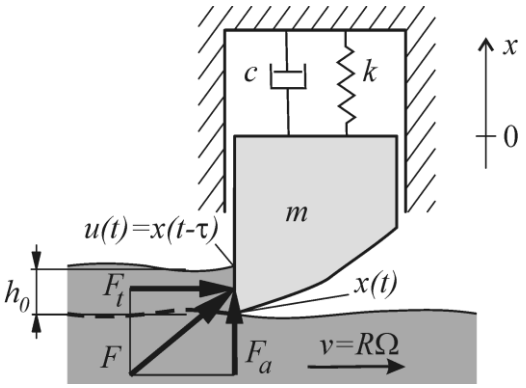

Figure 1: Mechanical model of the turning process with surface regeneration effect

The governing equation of the simplest, 1DoF turning model is given with [Tlusty and Polácek, 1963] [Tobias, 1965]:

$$m\ddot{x}(t) + c\dot{x}(t) + kx(t) = F_a, \tag{1}$$

where F_a is the cutting force in axial direction. The mechanical model can also be well characterized by its frequency response function (FRF) H_1, as follows

$$x(\omega) = H_1(\omega)F_a. \tag{2}$$

H_1 is usually determined by modal testing.

The axial cutting force is influenced by the variation of the tool motion, but is constant, if there is no vibration. However, for stability analysis only the variation of the axial cutting force and the tool motion around the stationary state is relevant.

According to the surface regeneration effect, the F_a depends on the current $x(t)$ and the previous $x(t-\tau)$ tool position, which describes the current surface profile $u(t) = x(t-\tau)$, where the time delay τ is determined with the help of the spindle speed Ω by $\tau = 2\pi/\Omega$.

If we consider that the variation of the force can be separated into two parts, one related to the current tool deflection and the other to the current surface profile:

$$F_a\big(x(t), u(t)\big) = F_x\big(x(t)\big) + F_u(u(t)). \tag{3}$$

If linearity is assumed, the variation of the axial cutting force due to a small perturbation in x(t) or in u(t) can be rewritten in frequency domain:

$$F_x\big(x(\omega)\big) = G_x(\omega)x(\omega), \tag{4}$$

$$F_u\big(u(t)\big) = G_u(\omega)u(\omega) = G_u(\omega)x(\omega)e^{-\mathrm{i}\omega\tau}, \tag{5}$$

where we denote the Force-FRFs with $G_x(\omega)$ and $G_u(\omega)$, which give back the force-output for a given input position.

3. DETERMINATION OF THE STABILITY CHART

For known $G_x(\omega)$ and $G_u(\omega)$ functions, stability analysis can be carried out. Substituting (4) and (5) into the perturbed governing equation (1) one obtains the following:

$$x(\omega) = H_1(\omega)\big(G_x(\omega) + G_u(\omega)e^{-\mathrm{i}\omega\tau}\big)x(\omega). \tag{6}$$

Finally, the stability boundary can be found based on the characteristic equation [Stépán,1989] ,[Merdol and Altintas, 2004]:

$$D = \Big(1 - H_1(\omega)\big(G_x(\omega) + G_u(\omega)e^{-\mathrm{i}\omega\tau}\big)\Big) = 0. \tag{7}$$

The real and the imaginary parts of Eq. (7) form a co-dimension 2 problem ($\mathrm{Re}(D) = 0, \mathrm{Im}(D) = 0$) in the usual parameter space of spindle speed Ω, depth of cut w and chatter frequency ω. This set of equations can be solved by the Multi-Dimensional Bisection Method (MDBM) [Bachrathy and Stepan 2012] for given Force-FRF functions, which are determined in the following section.

4. THEORETICAL FORCE-FRF

With the well-known proportional force model [Tlusty and Polácek, 1963] [Tobias, 1965]

$$F_a = k_1 w(h_0 - x(t) + x(t-\tau)), \tag{8}$$

the two Force-FRFs are:

$$G_x(\omega) = -k_1 w\,, \qquad G_u(\omega) = -G_x(\omega) = k_1 w\,. \tag{9}$$

The corresponding Bode-plots can be seen in Fig. 2.a), and the stability diagram together with the robust stability limit, which forms the lower envelope of the stability lobe structure [Bachrathy 2015] are presented in Fig. 2.b).

4.1 Process damping model

The force model including the process damping effect can be written in the following form [Budak and Tunc, 2009], [Chiou et al., 1998]:

$$F_a = k_1 w(f_z - x(t) + x(t-\tau)) - Cw\tau\dot{x}(t), \qquad (10)$$

where C is the process damping coefficient. For the Force-FRFs, this leads to:

$$G_x(\omega) = -k_1 w - i\,\omega\, Cw\,\tau\,, \qquad G_u(\omega) = k_1 w. \qquad (11)$$

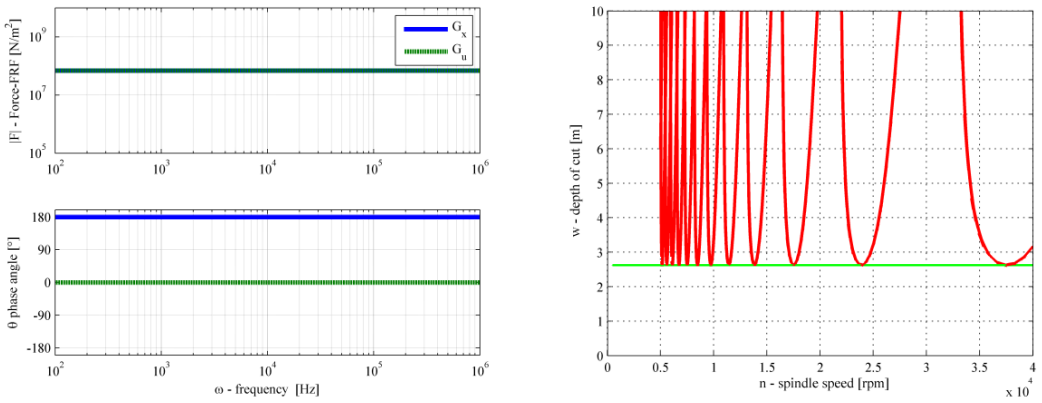

Figure 2: (a) Force-FRF for proportional cutting force model (blue continuous: G_x, greed dotted: G_u)
(b) The corresponding stability chart (red: stability limit, green: robust stability limit)

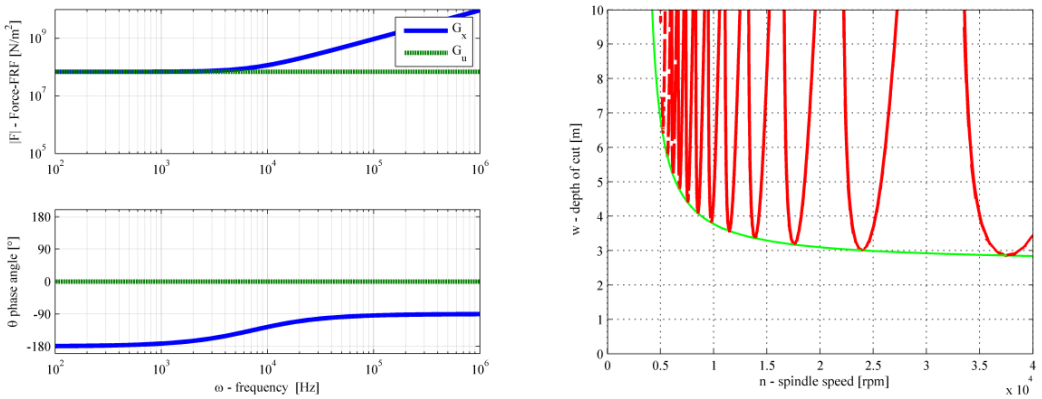

Figure 3: (a) Force-FRF for cutting force model with process damping
(blue continuous: G_x, greed dotted: G_u)
(b) The corresponding stability chart (red: stability limit, green: robust stability limit)

4.2. Short-delay model

The short-delay model is described in details in [Stépán,1989], where F_f is given in the following integral form with distributed time-delay:

$$F_a = k_1 w \int_0^{\theta_{max}} \gamma(\theta)(h_0 - x(t-\theta) + x(t-\tau-\theta))\mathrm{d}\theta. \qquad (12)$$

After straightforward calculations one ends up with:

$$G_x(\omega) = -k_1 w \int_0^{\theta_{\max}} \gamma(\theta)\left(e^{-\mathrm{i}\omega\theta}\right)\mathrm{d}\theta\,, \qquad G_u(\omega) = -G_x(\omega). \qquad (13)$$

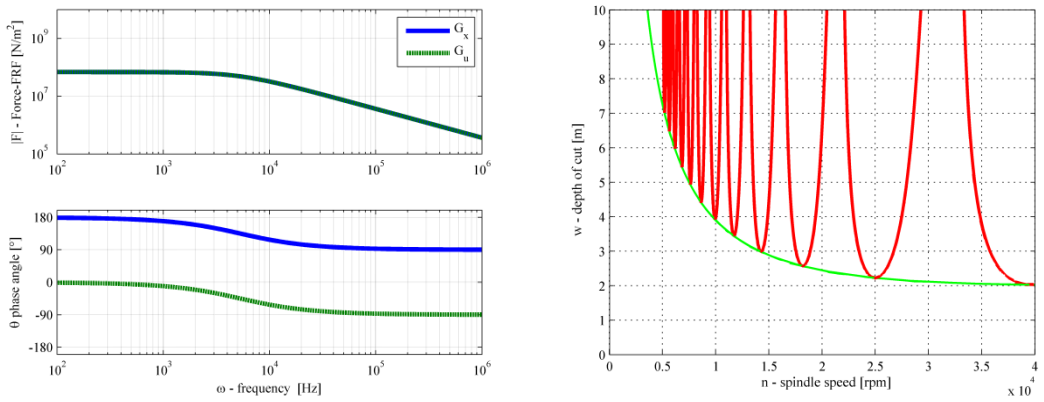

Figure 4: (a) Force-FRF of the short-delay cutting force model (blue continuous: G_x, greed dotted: G_u) (b) The corresponding stability chart (red: stability limit, green: robust stability limit)

It is important to note, that even though the magnitudes of the Force-FRFs given by the process damping and the short-delay force models are very different, both describe the shift of the lobes for the low spindle speed range in a similar way. It seems, that it is not the force magnitude, but the phase shift of the force, which has a key-role, even though they are not the same for the two models.

In order to capture the relevant sources of the lobe-shifting effect, such as contact forces on the flank face, short regenerative effect on the rake face, and plastic deformation, thermal effects at the tool tip, FEM simulations are carried out.

5. FINITE ELEMENT SIMULATION

5.1. Material model

The material model adopted in this study is based on an elastic-viscoplastic constitutive equation extended with thermal softening effect, where the yield stress of the material is governed by the expression proposed by Johnson and Cook [Johnson & Cook, 1985]:

$$\bar{\sigma} = \left(A + B \cdot \left(\bar{\varepsilon}^{\mathrm{pl}}\right)^{n}\right) \cdot \left(1 + C \cdot \ln\left(\frac{\dot{\bar{\varepsilon}}^{\mathrm{pl}}}{\dot{\varepsilon}_0}\right)\right) \cdot \left(1 - \left(\frac{T - T_r}{T_m - T_r}\right)^{m}\right), \tag{14}$$

where $\bar{\sigma}$ represents the yield stress, $\bar{\varepsilon}^{\mathrm{pl}}$ is the accumulated equivalent plastic strain, $\dot{\bar{\varepsilon}}_0$ denotes the reference strain rate, T is the current temperature, whereas T_r and T_m are the reference and the melting temperature. Constants A, B, C, n and m are material parameters. Equation (14) is a built-in model in ABAQUS. The material parameters for the A2024-T351 workpiece are collected in Table 3. [Mabrouki et al., 2008].

Table 1: Material parameters for the Johnson-Cook plasticity model

A[MPa]	B[MPa]	n[-]	C[-]	m[-]
352	440	0.42	0.0083	1

The material damage is governed by the Johnson-Cook shear failure model, where the damage initiation law is specified by the relation for the equivalent plastic strain of the damage initiation:

$$\bar{\varepsilon}_{0i}^{\mathrm{pl}} = \left(D_1 + D_2 \cdot \exp\left[D_3 \cdot \frac{p}{\bar{\sigma}} \right] \right) \cdot \left(1 + D_4 \cdot \ln\left[\frac{\dot{\bar{\varepsilon}}^{\mathrm{pl}}}{\dot{\bar{\varepsilon}}_0} \right] \right) \cdot \left(1 + D_5 \left(\frac{T - T_r}{T_m - T_r} \right) \right), \qquad (15)$$

where $\left(p / \bar{\sigma} \right)$ is the stress triaxiality and $D_1 \ldots D_5$ are additional material parameters, and the values for A2024-T351 are reported in Table 2. [Mabrouki et al., 2008]. Additional material and physical parameters for the given material are listed in Table 3. [Mabrouki et al., 2008].

5.2. Geometry, mesh and loading conditions

The geometry of the workpiece is depicted in Fig. 5, where the dimensions are to be understood in [mm].

For sake of simplicity, the tool is modeled as a rigid body with rake and clearance angles 0° and 20°, respectively.

Table 2: Failure parameters for A2024-T351

D_1 [-]	D_2 [-]	D_3 [-]	D_4 [-]	D_5 [-]
0.13	0.13	-1.5	0.011	0

Table 3: Workpiece material and physical parameters

Density $\left[\mathrm{kg/m^3}\right]$	Young's modulus $\left[\mathrm{GPa}\right]$	Poisson's ratio $\left[-\right]$	Specific heat $\left[\mathrm{J/kg/°C}\right]$
2700	73	0.33	$0.557T + 877.6$
Thermal conductivity $\left[\mathrm{W/m/°C}\right]$	Thermal expansion $\left[\mu\mathrm{m/m/°C}\right]$	T_m $\left[\mathrm{°C}\right]$	T_r $\left[\mathrm{°C}\right]$
$25 \le T \le 300$: $0.247T + 114.4$ $300 < T \le T_m$: $0.125T + 226$	$8.9 \times 10^{-3} T + 22.2$	520	25

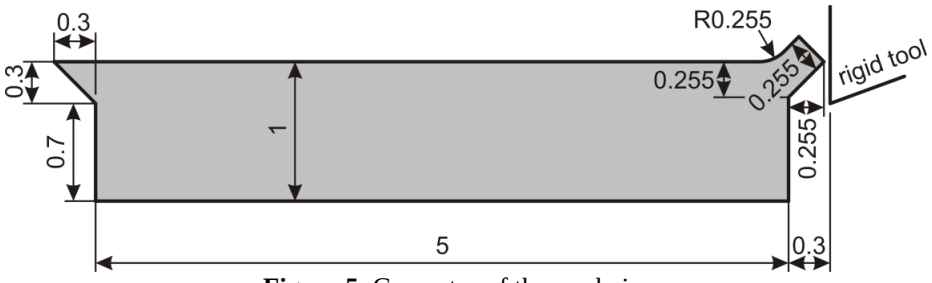

Figure 5: Geometry of the workpiece

The applied element type is CPE4RT, 4-node plane strain thermally coupled quadrilateral element with reduced integration and hourglass and distortion control. The applied element size is 0.015mm.
The applied cutting speed of the tool along the horizontal direction is 5 m/s.

CASE 1 - Perturbation in the tool path:
In FEM simulations, the impact-like motion is difficult to model, hence a smoothed step function will be used. The perturbation in vertical direction is controlled by the ABAQUS built-in „*Smooth Step*" amplitude function with the tabular data provided in Table 4. The displacement perturbation in vertical direction is 0.045 mm. The initial dept-of-cut was 0.3 mm. The path of the tool in the neighboring region of the perturbation is illustrated in Fig. 6, where the dimensions are given in [mm].

Table 4: Tabular data for the smooth step function

Time	Amplitude
0	0
0.00028	0
0.0002925	1
0.00053	1

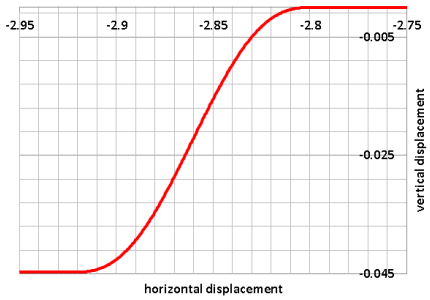

Figure 6: Loading path in the region of the perturbation

CASE 2 - Perturbation in the workpiece surface contour: In this case, the contour of the workpiece $u(t)$ is changing at time 0.00028 s according to Fig.7.

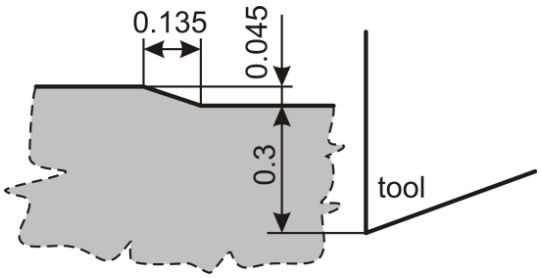

Figure 7: Loading path in the region of the perturbation

The friction coefficient defined between the tool and the material was 0.1. The maximum contact shear stress allowed in this simulation was $A/\sqrt{3}$. The default heat generation option was set for the contact property. In addition, the default value 0.9 was used for the inelastic heat generation for the workpiece material.

5.3. Results

For illustration purposes, the distribution of the Mises equivalent stress and the nodal temperature corresponding to CASE 1 is demonstrated in Fig. 8 at step time 2.26E-04. The variation of the vertical force acting on the tool is shown in Fig 9.

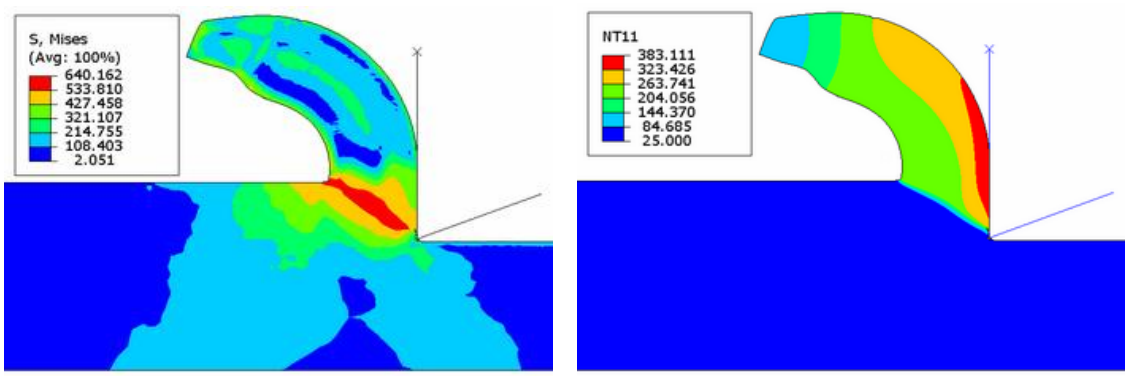

Figure 8: Distribution of the Mises equivalent stress and the nodal temperature

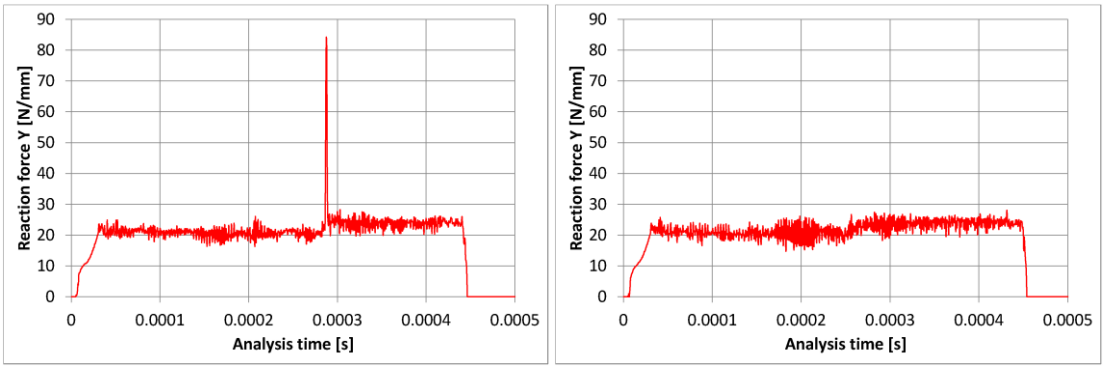

Figure 9: Vertical force acting on the tool in CASE 1 and in CASE 2, respectively

5.4. FEM based Force-FRFs

Based on the predefined tool path and on the resultant force fluctuation the Force-FRFs can be determined with

$$G_x(\omega) = w\frac{F_x^{FEM}(x(\omega))}{x^{FEM}(\omega)}, \qquad G_u(\omega) = w\frac{F_u^{FEM}(x(\omega))}{u^{FEM}(\omega)}. \tag{16}$$

The multiplication with w is necessary hence only plane strain elements were used. The resultant raw Force-FRFs are plotted in Fig.10 a) and the filtered ones in Fig.10 b).

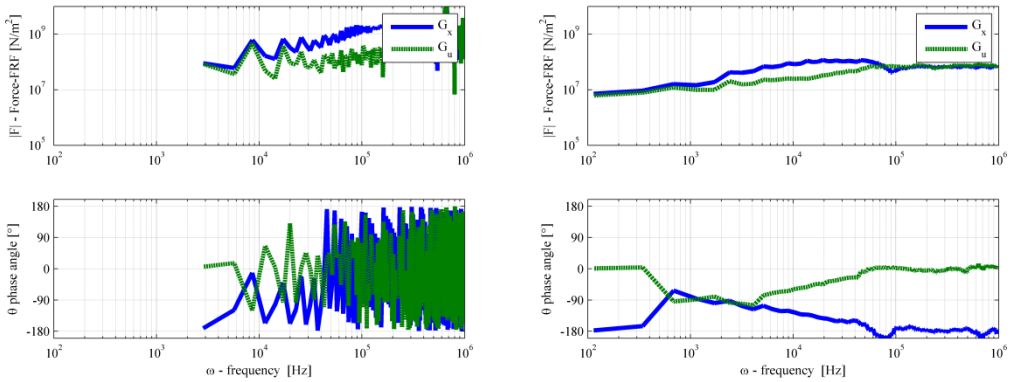

Figure 10: Force-FRF based on the FEM simulations (blue: continuous: G_x, greed dotted: G_u)
(b) The corresponding stability chart (red: stability limit, green: robust stability limit)

Due to difficulties of numerical calculations, large fluctuations can be observed in the force functions, which leads to moderate noise in the Force-FRFs' magnitudes and to large noise in their phase angles. With proper filtering techniques, the tendencies can be visualized. On one hand, concerning the magnitudes, it shows correlation with the process damping force model, which has its roots in the compressed workpiece material appearing in the FEM simulation due to high velocity of the perturbed tool motion. On the other hand, the changing phase angle in both Force-FRF functions prevail characteristic of the short-delay force model.

In order to determine stability charts based on these Force-FRF functions, higher time resolution and much smaller element size are required.

6. CONCLUSION

With the introduced Force-FRF formulation the conditions of the stability computation can be given in a simple form, even for force models including distributed delays.

In order to capture all relevant sources of lobe-shifting phenomenon, such as contact forces on the flank face, short regenerative effect on the rake face, and also plastic deformation, thermal effects at the tool tip, FEM simulations were carried out.

Future goal is to create FEM computation with higher resolution to be able to determine the corresponding stability charts and to determine the Force-FRFs via direct measurements.

ACKNOWLEDGMENT

The work was supported by the János Bolyai Research Scholarship of the Hungarian Academy of Science and by the Hungarian Scientific Research Fund under grant OTKA PD112983 and K101714. The research leading to these results has received funding from the European Research Council under the European Union's Seventh Framework Programme (FP/2007-2013) / ERC Advanced Grant Agreement n. 340889.

REFERENCES

[Altintas et al., 2008] Altintas, Y., Eynian, M., Onozuka , H.; *"Identification of dynamic cutting force coefficients and chatter stability with process damping"*; CIRP Annals - Manufacturing Technology; 57(1), 2008, pp. 371-374.

[Bachrathy 2015] Bachrathy, D., "*Robust stability limit of delayed dynamical systems*"; Periodica Polytechnica. Mechanical engineering, 2015, (submitted)

[Bachrathy and Stepan 2012] Bachrathy, D., and Stepan, G., "*Bisection method in higher dimensions and the effciency number*"; Periodica Polytechnica. Mechanical engineering, 2012, 56(2), 81-86.

[Budak and Tunc, 2009] Budak, E., Tunc, L. T.; *"A New Method for Identification and Modeling of Process Damping in Machining"*; Journal of Manufacturing Science and Engineering; 2009, 131(5) p.10.

[Budak and Tunc, 2010] Budak, E., Tunc, L. T.; *"Identification and Modeling of Process Damping in Turning and Milling Using a New Approach"*; CIRP Annals Manufacturing Technology; 2010, 59(1) p.6.

[Chiou et al., 1998] Chiou, Y. S., Chung E. S., Liang S. Y.; *"Analysis of tool wear effect on chatter stability in turning"*; International Journal of Mechanical Sciences; 37(4), 1995, pp. 391-404.

[Das and Tobias, 1967] Das, M.K., Tobias, S.A.; *"The Relation Between the Static and the Dynamic Cutting of Metals"*; International Journal of Machine Tool Design and Research; 7, 1967, pp. 63–8.

[Eynian, 2010] Eynian, M.; PhD Thesis; *"Chatter Stability of Turning and Milling with process Damping"*; University of British Columbia;2010.

[Johnson & Cook, 1985] JOHNSON, G.R. AND COOK, W.H.; "Fracture characteristics of three metals subjected to various strains, strain rates, temperatures and pressures"; *Engineering Fracture Mechanics*, **21**, 31-48 (1985)

[Mabrouki et al., 2008] MABROUKI, T. AND GIRARDIN, F. AND ASAD, M. AND RIGAL, J-F..; "Numerical and experimental study of dry cutting for an aeronautic aluminium alloy (A2024-T351)"; *International Journal of Machine Tools & Manufacture*, **48**, 1187-1197 (2008)

[Merdol and Altintas, 2004] Merdol, S. D.; Altintas, Y.; *"Multi Frequency Solution of Chatter Stability for Low Immersion Milling"*; Journal of Manufacturing Science and Engineering; 2004, 126(3), pp. 459-467.

[Stépán, 1984] Stepan, G.; *"A stability criterion for retarded dynamical systems"*, Zeitschrift für angewandte Mathematik und Mechanik 1984, 64, T345-T346.

[Stépán,1989] Stépán, G.; 1989; *"Retarded Dynamical Systems"*; Longman, Harlow.

[Tlusty and Polácek, 1963] Tlusty, J.; and Polácek, M.; *"The stability of machine-tool against self-excited vibration in machining";* In: Proceedings of the International Research in Production Engineering, American Society of Mechanical Engineers (ASME), p. 465.

[Tobias, 1965] Tobias, S.A.; 1965; *"Machine Tool Vibration"*; Blackie & Son, Ltd., London